



# Electrochemical performances of activated carbon prepared using eggshell waste

V. Balasubramanian<sup>1</sup> · T. Daniel<sup>1</sup> · J. Henry<sup>1</sup> · G. Sivakumar<sup>2</sup> · K. Mohanraj<sup>1</sup> Received: 9 October 2019 / Accepted: 18 December 2019 / Published online: 21 December 2019  
© Springer Nature Switzerland AG 2019

## Abstract

This paper describes the preparation of activated carbon (Ac) from broiler hen eggshell (BES) and Country hen eggshell (CES) waste with the assistance of chemical activating agent orthophosphoric acid ( $H_3PO_4$ ) and eggshell powder for 4:1 and 4:2 concentrations. XRD analysis affirmed the formation of Ac and the hexagonal structure of  $CaCO_3$  for both BES and CES samples. The average crystalline size, dislocation density, microstrain, lattice parameter, and cell volume values are found to be higher for CES. The FTIR spectra confirmed the presence of functional groups of BES and CES samples of Ac. UV-DRS spectra exhibited strong absorption in the visible region for BES and the bandgap value is found to be around 1.2 eV for both BES and CES. The surface morphology reveals the porous nature, irregular shape and uniform size particles of Ac. Cyclic voltammetry and electrochemical impedance spectroscopy measurements were performed to study the energy storage application. Though both BES and CES have showed the capacitive behavior, the sample BES exhibit higher specific capacitance of 155.8 F/g is achieved for BES than CES. Similarly, the  $R_s$  and  $R_{ct}$  values are calculated from the impedance measurement and it is found to be lower for BES sample that indicates improved electrical conductivity.

**Keywords** Activated carbon · Eggshell · Ortho-phosphoric acid · Specific capacitance

## 1 Introduction

Activated carbon (Ac) being a carbonaceous material, predominantly amorphous in nature and has high porosity due to the production and treatment. In the recent years, the use of agricultural waste biomass such as waste coffee beans [1], cassava peel waste [2], bamboo waste [3], sugarcane bagasse [4, 5], rice husk [6], peanut shell [7], rubberwood, saw dust [8] act as a precursor material to prepare porous carbon for electric double layer capacitors (EDLC) due to their abundant availability and low cost. The large amount of egg waste creates an environmentally and economically challenging problem if it is not managed suitably [11]. Moreover, activated carbon has special features like absorption of heavy metal ion and organic pollutants which results in increased antibacterial effect.

The eggshell's composition consists of calcium carbonate (94%), calcium phosphate (1%), magnesium carbonate (1%), organic substances (4%) [12]. Bio derived activated carbon-based materials have been employed as a high performance supercapacitor applications due to their intrinsic and extrinsic characteristics such as high electronic conductivity, high surface area, low cost, affordability to large scale applications. Zhang et al. [9] achieved a high energy density supercapacitor of 17.2 and 87.8 Wh/kg in both acidic and organic electrolytes for nitrogen doped commercial activated carbon. Bhomick et al. [10] reported both experimental and theoretical investigation of KOH synthesized activated carbon using Schima wallichii biomass by varying the carbonization temperature. Sivachidambaram et al. [11] prepared activated carbon-based electrode material from the *Borassus flabellifer*

✉ K. Mohanraj, kmohanraj.msu@gmail.com; mohanraj@msuniv.ac.in | <sup>1</sup>Department of Physics, Manonmaniam Sundaranar University, Tirunelveli, Tamil Nadu 627 012, India. <sup>2</sup>CISL, Department of Physics, Annamalai University, Annamalai Nagar, Tamil Nadu 608 002, India.



flower for analyzing supercapacitor behavior. Li et al. [12] prepared carbonized chicken eggshell membrane with 3D architecture as high performance electrode materials for supercapacitors. Meng et al. [13] has investigated supercapacitor behavior of waste eggshell used as reactor and template for synthesis of  $\text{Co}_9\text{S}_8$  nanorod arrays on carbon fibers for energy storage. Jose et al. [14] fabricated highly flexible hierarchical polypyrrole/carbon nanotube on eggshell membranes for supercapacitors and calculated that the areal capacitance of  $564.5 \text{ mF/cm}^2$  and volumetric capacitance of  $24.8 \text{ F/cm}^3$  respectively. Pingping et al. [15] prepared biowaste-derived three-dimensional porous network carbon and bio separator and achieved high-performance asymmetric supercapacitive performance ( $478.5 \text{ F/g}$ ) at a current density of  $500 \text{ mA/g}$ . Therefore, it is observed from the literature that the utilization of eggshell waste for generating activated carbon is not explored well and there is a paucity of reports on this material. Hence, it is motivated to synthesis activated carbon from eggshell waste as a precursor material for energy storage application.

## 2 Experimental methods

### 2.1 Preparation of activated carbon

Generally, eggshell is varied depends on the type of hen. Here we have taken two different kinds of eggshell; broiler hen and Country hen eggshell named as BES and CES were collected separately from the residential wastes. First, the shells were washed with distilled water several times to remove the impurities. Then they were air dried and ground using a mortar to get the finely powdered sample. The powder sample was taken in the crucible and placed in an oven for 6 h at  $110 \text{ }^\circ\text{C}$ . The obtained product was chemically activated using  $\text{H}_3\text{PO}_4$  (orthophosphoric acid), in which the sample was soaked for 24 h. The sample BES and CES were prepared by mixing 4% of  $\text{H}_3\text{PO}_4$  with 1% of activated carbon for 4:1 and 4% of  $\text{H}_3\text{PO}_4$  with 2% of activated carbon for 4:2 respectively. The precursor solution was stirred well for 2 h. Then pour it for filtration and the collected samples were again dried at  $110 \text{ }^\circ\text{C}$  for 24 h in oven followed by heating at  $550 \text{ }^\circ\text{C}$  for 2 h. The powder was rinsed using 1 M of conc. HCl and distilled water to remove residual inorganic matter. Finally, the activated carbon is obtained and stored for further investigations.

### 2.2 Characterization technique

The structural property of the activated carbon was characterized using XPERT-PRO diffractometer system with a characteristic wavelength of  $1.5406 \text{ \AA}$  for the Ka

radiation. XRD was recorded using PANalytical X'Pert Pro diffractometer with tube voltage of 30 kV and the current 40 A. The presence of various functional groups was identified from the Perkin Elmer—spectrum two Fourier transform infra-red (FTIR) spectrometer in the range  $4000\text{--}400 \text{ cm}^{-1}$ . The surface morphology study was carried out using EVO18 (CARL ZEISS) scanning electron microscope. The optical bandgap of the samples was calculated from the reflectance spectra (DRS) recorded using UV–visible spectrophotometer (Shimadzu UV 2600) in the wavelength region  $220\text{--}850 \text{ nm}$  and  $\text{BaSO}_4$  were used as reference. The electrochemical measurements were performed in the conventional three-electrode system using CH1604E electrochemical workstation. Here,  $0.5 \text{ M H}_2\text{SO}_4$  was used as the electrolyte, while the working electrodes were prepared by mixing the electroactive material with polyvinyl alcohol and coated in a stainless steel substrate with an exactly  $1 \text{ cm}^2$  active area. A large surface area platinum mesh and Ag/AgCl electrode were used as counter and reference electrode respectively. The electrochemical performances of the fabricated electrode were characterized by cyclic voltammetry (CV) and electrochemical impedance spectroscopy (EIS) measurements. The CV curves were recorded at various scan rates ( $10, 50, 100$  and  $200 \text{ mV/s}$ ) in a potential window of  $-1.5$  to  $+1.5 \text{ V}$ . The EIS measurements were carried out in the frequency range of  $0.1 \text{ Hz}$  to  $100 \text{ kHz}$  with an AC amplitude of  $5 \text{ mV}$ .

Proximate analysis of activated carbon was determined according to Ekpete et al. [16].

#### (i) Ash content

Ash content is the measure of the mineral oxide content of activated carbon on a weight basis. It is measured by converting the mineral oxides to the respective oxides at  $800 \text{ }^\circ\text{C}$ .

$$\left\{ (M_c + M_a) - M_c / (M_c + M_s) - M_c \right\} \times 100$$

where  $M_c$  is the mass of the crucible,  $M_a$  is the mass of the ash,  $M_s$  is the mass of the sample.

#### (ii) Moisture content

The moisture content of activated carbon is measured as weight loss after heating at  $150 \text{ }^\circ\text{C}$  and allowed to dry to a constant weight.

$$(W_w - W_d / W_w) \times 100$$

where  $W_w$  is the amount of sample before drying,  $W_d$  is the amount of sample after drying.

#### (iii) Specific gravity

The relative density bottles were cleaned, dried and weighed empty. One-third of the activated carbons were put into it and weighed again. The relative density bottles were filled with water and reweighed. Finally, the bottles were emptied, cleaned of the activated carbon particles filled with water alone and weighed.

(iv) Bulk density

A cylinder and an aluminium plate were each weighed. A sample of activated carbon was put into the cylinder and reweighed. The samples were transferred into the aluminium plate and put into an oven so as to dry it to constant weight at a temperature of 105 °C for 1 h. The weight of the dried samples was taken again after drying. A clean dry well-corked density bottle was weighed.

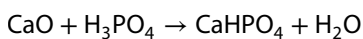
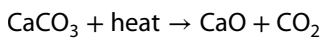
$$\text{Bulk density} = \text{Mass of wet sample} / \text{mass of volume}$$

### 3 Result and discussion

From the proximate analysis, the total ash content, moisture content, specific gravity and bulk density for BES and CES in given in Table 1 for comparison.

From the table, it is observed that all the physical parameters were matched with the commercial activated carbon [16]. Hence, it is affirmed the presence of activated carbon along with CaCO<sub>3</sub>.

The X-ray diffraction pattern of grounded cum heated hen eggshell (BES) at 110 °C is shown in Fig. 1. The reaction mechanism can be understood by the following equations:



In the diffraction pattern, a prominent and high intense crystalline peak appears at 2θ = 29.66° belongs to 110 plane of hexagonal structure of carbon (JCPDS: 460943) and the remaining crystalline peaks at 2θ = 23.66°, 2θ = 29.54°, and 2θ = 36.28° belongs to the rhombohedral structure of CaCO<sub>3</sub> (JCPDS: 050586). In the case of H<sub>3</sub>PO<sub>4</sub> activated samples (4:1), the major crystalline peaks appears at 2θ = 29.25° and 2θ = 31.04° belongs to the hexagonal structure of carbon and these peaks are

**Table 1** Proximate analysis of BES, CES and activated carbon

S. no.	Parameter	BES	CES	Activated carbon
1.	Total ash content	2.3%	1.8%	17.1%
2.	Moisture content	10%	8.3%	16.67%
3.	Specific gravity	0.54	0.63	1.8
4.	Bulk density (g/cm <sup>3</sup> )	0.57	0.64	0.66

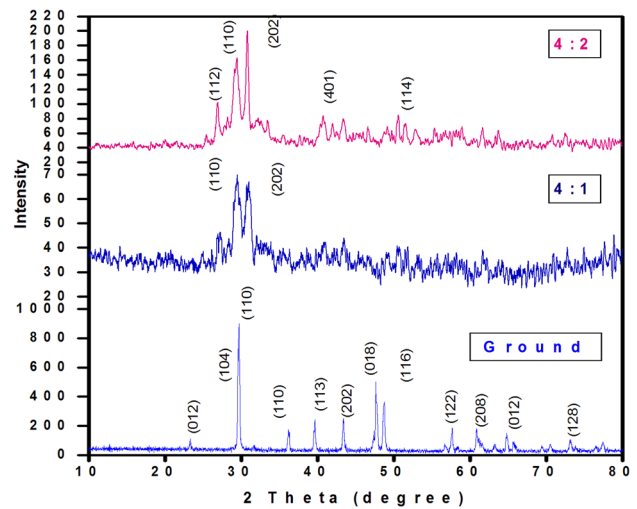


**Fig. 1** XRD pattern of Ac received from grounded, 4:1 and 4:2 concentration of BES

slightly shifted in 4:2 concentration from 2θ = 29.25° and 2θ = 31.04° to 2θ = 29.30° and 2θ = 30.77°. This may be attributed to the increase the H<sub>3</sub>PO<sub>4</sub> content associated with the biochemical content variation in the eggshell waste [17]. The non-existence of majority of the activated carbon peaks related to CaCO<sub>3</sub> in the patterns suggests that carbon fibers exhibit less activation in 4:1 and 4:2 concentration, which could be attributed to the relatively low carbonization temperature of 550 °C.

In the case of CES (Fig. 2), the XRD pattern of the grounded CES sample seems to be similar to that of BES with a slight variation in the intensity. On H<sub>3</sub>PO<sub>4</sub> activation, the crystalline peaks of CES (4:1 concentration) are

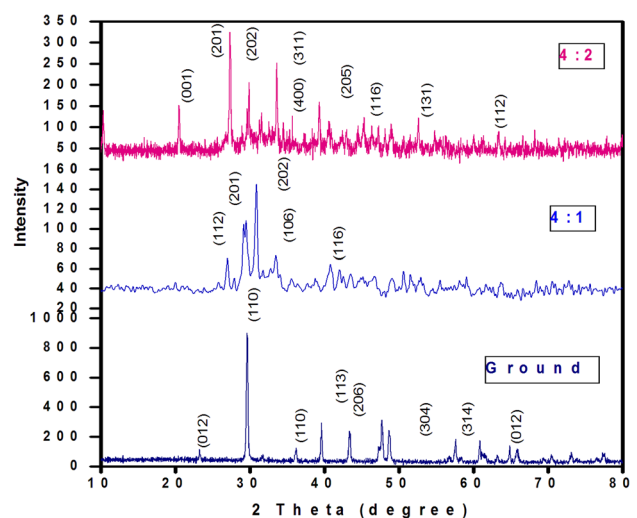


**Fig. 2** XRD pattern of Ac received from grounded, 4:1 and 4:2 concentration of CES

well-matched with Carbon (JCPDS: 460943) and the major crystalline peak appears at  $2\theta = 29.85^\circ$  belongs to 110 plane. Similarly, carbon peaks are observed at  $2\theta = 33.59^\circ$ ,  $2\theta = 34.49^\circ$ , and  $2\theta = 39.37^\circ$  for 4:2 concentration and remaining peaks belongs to  $\text{CaCO}_3$ . By comparing the both BES and CES, the samples prepared using 4:1 concentration is well agreed with carbon and further increase the concentration (4:2), leads to the formation of  $\text{CaCO}_3$  for both BES and CES as may be attributed to type of eggshell and thermal energy produced strain in the sample. The intensity and broadening of the peaks are almost identical in BES and CES samples. The result agrees well with the earlier report on activated carbon from eggshell membranes prepared using sodium acetate and zinc metal activation [18].

The average crystallite size of both ground cum heated samples and activated samples were calculated using Scherrer formula [19] given by

$$D = 0.9\lambda / \beta \cos\theta \tag{1}$$

The strain ( $\epsilon$ ) and dislocation density ( $\delta$ ) of the Eggshell samples were calculated using the formula given by

$$\epsilon = \beta / \tan\theta \tag{2}$$

$$\delta = 1/d^2 \tag{3}$$

The lattice parameter and cell volume value were calculated using unit cell software and their results are tabulated in Table 2. It is noticed that the crystalline size, dislocation density, microstrain, lattice parameter, and cell volume values are higher for CES which may be attributed to the type of the samples.

The FTIR spectra of raw-cum heated samples are shown in Fig. 3. By comparing the vibrational spectra, the position of the bands/peaks are identical to each other, however, its variation in intensity is observed and are summarized in Table 3. In both BES and CES, a broad and strong peak is observed at  $1420\text{ cm}^{-1}$  and a sharp peak appears at  $870\text{ cm}^{-1}$  due to stretching and bending vibration of

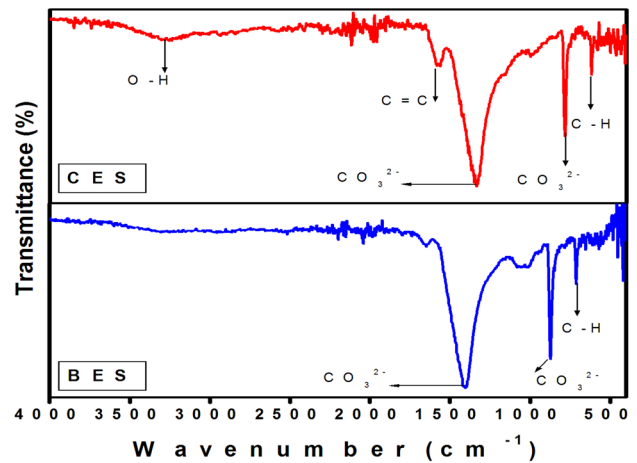


Fig. 3 FTIR spectra of grounded BES and CES samples

carbonate group present in the sample [20, 21]. In addition, the characteristic peak of carbon is found around  $1630\text{ cm}^{-1}$  belongs to C=C vibration.

Figure 4a, b shows the FTIR spectra of Ac BES and CES for 4:1 and 4:2 concentration respectively. It is important to notice that the sharp peaks that appeared at  $870\text{ cm}^{-1}$  in the ground cum heated samples is disappeared in the activated samples. While a band appears around  $930\text{ cm}^{-1}$  with weak intense band at  $712\text{ cm}^{-1}$  which is due to the bending vibration of  $\text{CaCO}_3$ . In addition, the characteristic peak of carbon (C=C) vibration is observed around  $1631\text{ cm}^{-1}$  for both BES and CES samples. In the FTIR spectra of both BES and CES, a weak peak is observed around  $1128\text{ cm}^{-1}$  and  $1070\text{ cm}^{-1}$  is due to symmetric P-O stretching vibration of  $\text{PO}_3^{2-}$  group which is due to the activating agent used in the materials [22]. A small hump and a weak peak are observed at  $556\text{ cm}^{-1}$  and  $448\text{ cm}^{-1}$  due to the bending vibration of  $\text{PO}_4^{3-}$  respectively [23]. By comparing the spectra, the vibrational spectra of CES are changed in terms of variation in intensity of the bands that may be due to the presence of protoporphyrin IX pigment present in CES. It is clearly revealed from the FTIR analysis that

Table 2 Crystalline size, dislocation density, micro strain, lattice parameter, cell volume

S. no.	Concentration	Resource material	Crystalline size ( $\times 10^{-9}\text{ m}$ )	Dislocation density ( $\times 10^{14}\text{ lines m}^{-2}$ )	Micro strain ( $\times 10^{-4}$ )	Lattice parameter		Cell volume, $V\ (\text{\AA})^3$
						a ( $\text{\AA}$ )	c ( $\text{\AA}$ )	
1.	Grounded Sample	BES	58	5	2.85	4.89	17.74	368.02
		CES	48	6	6.33	7.19	17.00	759.40
2.	4:1	BES	6	1	3.48	7.08	17.09	742.88
		CES	23	75	25.95	7.10	17.05	760.49
3.	4:2	BES	20	9	6.58	7.15	17.0	754.77
		CES	50	4	7.35	7.16	17.31	770.47

**Table 3** FTIR vibrational frequency assignment of BES and CES

S. no.	Band assignment	Observed frequency (cm <sup>-1</sup> )						Frequency
		Raw heated sample		4:1		4:2		
		BES	CES	BES	CES	BES	CES	
1	OH vibration	3366 <sub>w</sub>	3365 <sub>w</sub>	3366 <sub>bh</sub>	3366 <sub>b</sub>	3366 <sub>w</sub>	3367 <sub>b</sub>	3300–3500
2	C=C vibration	1656 <sub>w</sub>	1627 <sub>w</sub>	1631 <sub>w</sub>	1627 <sub>w</sub>	1619 <sub>w</sub>	1630 <sub>sp</sub>	1630
3	Vibration of carbonate	1420 <sub>sp</sub>	1420 <sub>sp</sub>	–	–	–	–	1417
4	Vibration of PO <sub>3</sub> <sup>2-</sup>	–	–	1071 <sub>w</sub>	1128 <sub>w</sub>	1074 <sub>w</sub>	1140 <sub>w</sub>	1120, 1042 and 1090
5	Vibration of CaCO <sub>3</sub>	–	–	934 <sub>w</sub>	916 <sub>w</sub>	928 <sub>w</sub>	–	924
	Vibration of P–O–P bending	–	–	–	–	–	946 <sub>w</sub>	943–980
6	Vibration of Carbonate	870 <sub>sp</sub>	870 <sub>sp</sub>	–	–	–	–	875
7	C–O stretching vibration of CO <sub>3</sub> <sup>2-</sup> group	712 <sub>w</sub>	712 <sub>w</sub>	712 <sub>w</sub>	712 <sub>w</sub>	712 <sub>w</sub>	712 <sub>w</sub>	715
8	Vibration of PO <sub>4</sub> <sup>3-</sup>	–	–	556 <sub>wh</sub>	550 <sub>h</sub>	563 <sub>wh</sub>	550 <sub>h</sub>	550–600
9	Vibration of O–P–O stretching Po <sub>4</sub> <sup>2-</sup> group	–	–	488 <sub>w</sub>	491 <sub>w</sub>	488 <sub>w</sub>	491 <sub>w</sub>	484

w weak, s strong, h hump, bh broad hump, wh weak hump, sp sharp peak

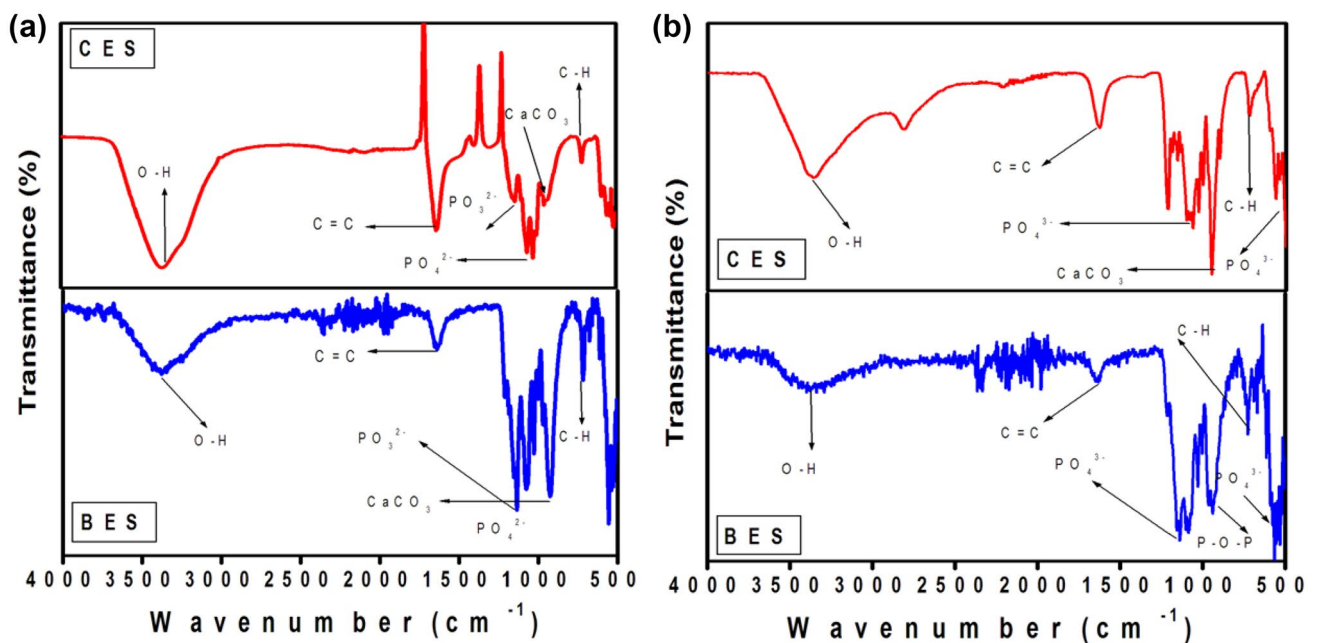


**Fig. 4** FTIR spectra of Ac from BES and CES for **a** 4:1 and **b** 4:2

the activation agent influenced the intensity of carbonyl bands in both eggshell samples.

### 3.1 SEM analysis

Figures 5 and 6 displays the scanning electron microscope (SEM) images of chemically activated BES and CES samples of activated carbon with different magnifications (5kx, 10kx, 20kx and 50kx). It can be seen from the images (BES) that the synthesized particles are highly agglomerated with porous nature which is irregularly distributed

over the surface as clearly shown in the higher magnification images (50kx). The porous nature may be attributed to the influence of activating agent H<sub>3</sub>PO<sub>4</sub> on eggshell. The advantage of the porous structure was that it will allow electrolyte penetration which is favorable for ion diffusion, charge transfer and capacitance increases [24, 25]. In the case of CES, the synthesized particles are flake-like structures and exhibit partial geometrical shape. But, the surface morphology is not dense compared to BES. It could be attributed to the type of eggs shells. This observation is in agreement with XRD and FTIR analysis. Generally

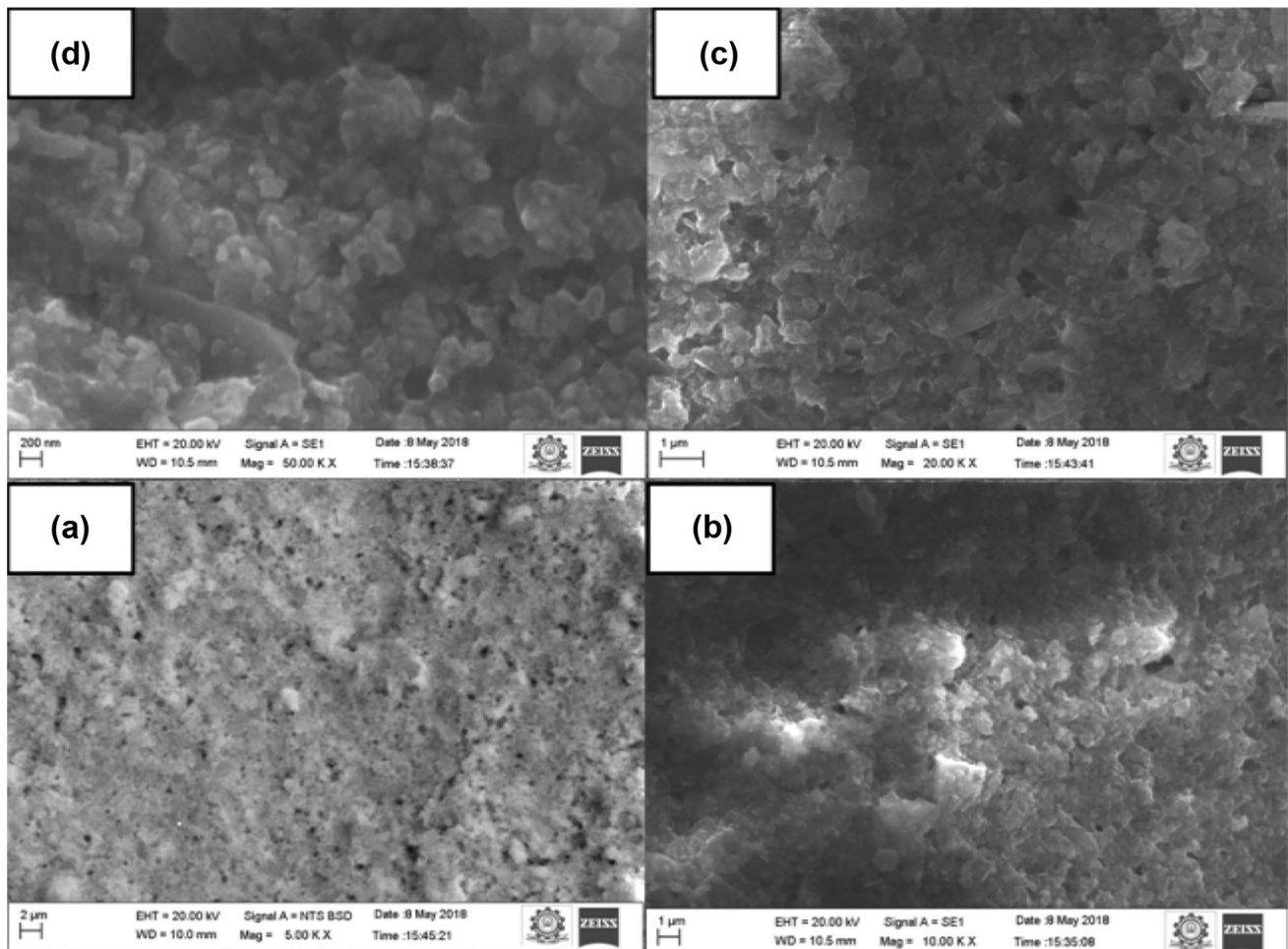


Fig. 5 SEM images of Ac from BES for 4:1 concentration

activated carbon synthesized using various biomaterials always show porous structure. In our study, we also received the porous structure of activated carbon for the BES sample. The high porosity results in increased charge storage characteristics which are in agreement with cyclic voltammetry study [26].

### 3.2 DRS analysis

Figure 7 shows the DRS spectra of activated carbon for 4:1 concentration (carbon:  $H_3PO_4$ ). It can be seen from the Fig. 7a that BES exhibited strong absorption in the visible region in comparison to CES. It could be attributed to the increase in the crystalline size of the BES particle (23 nm) [27, 28]. Usually bigger size crystallite has fewer grain boundaries, leading to less radioactive combination centers in the material. The reason for decrease the optical absorption in CES may be due to the increase in grain boundaries and defects which increases the maximum scattering of light. Figure 7b

shows Ac prepared for 4:2 concentration. By comparing the results, the DRS spectra of 4:2 are almost identical to the concentration of 4:1 and difficult to distinguish the performance of optical absorption as reflected in the band gap value. The bandgap was determined from the DRS using the Kubelka–Munk relation which is given by

$$F(R_{\infty}) = \frac{[1 - R_{\infty}]^2}{2R_{\infty}} \tag{4}$$

where  $F(R_{\infty})$  is the absorbance of the sample.

$$(R_{\infty}) = \frac{R_{sample}}{R_{standard}} \tag{5}$$

The bandgap (Fig. 8) is found to be around 1.2 eV for both BES and CES samples. Almost the closer value of bandgap of the egg samples are attributed to the increasing amount of chemical activator has finely altered the crystalline structure and morphology of

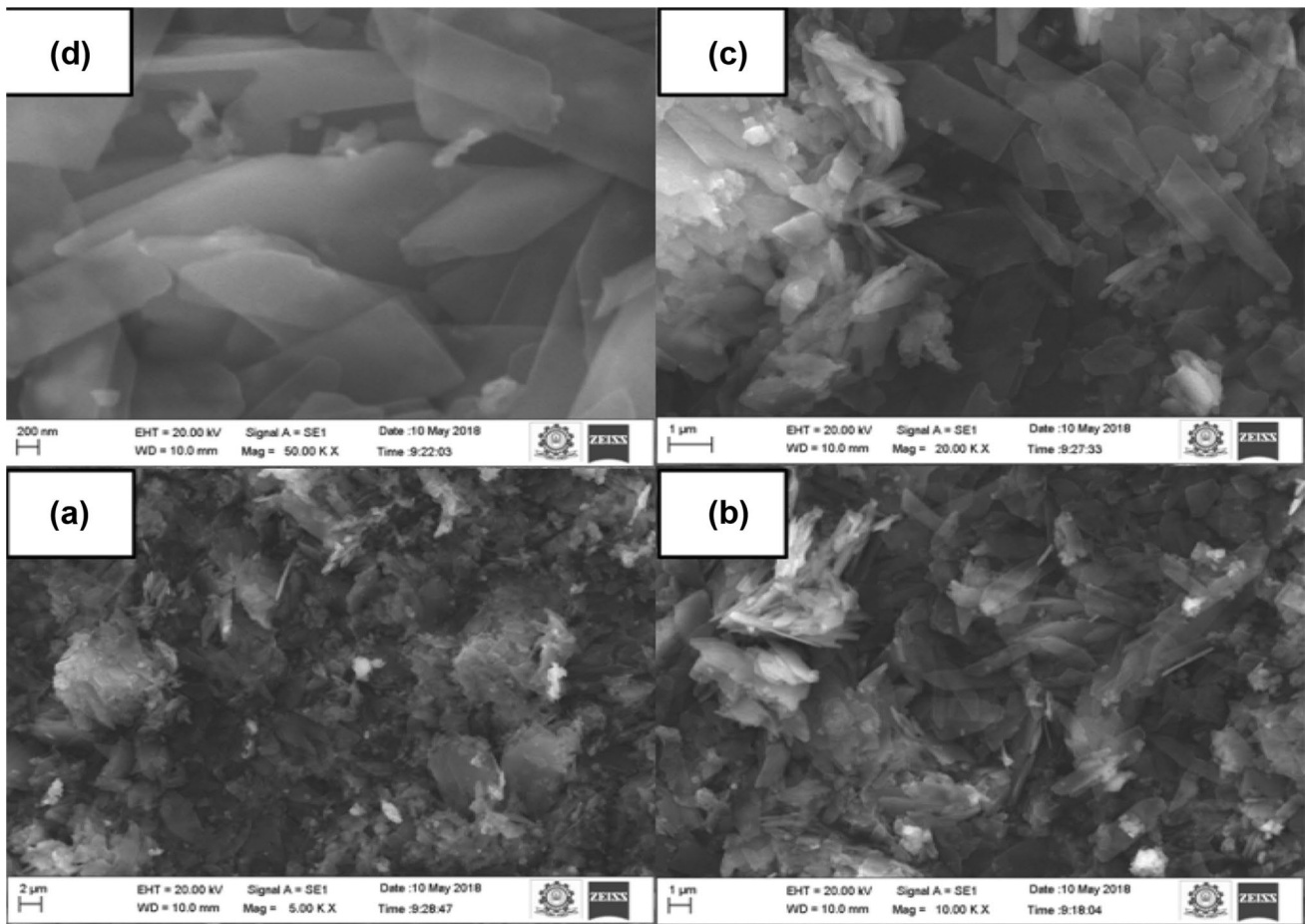


Fig. 6 SEM images of Ac from CES for 4:1 concentration

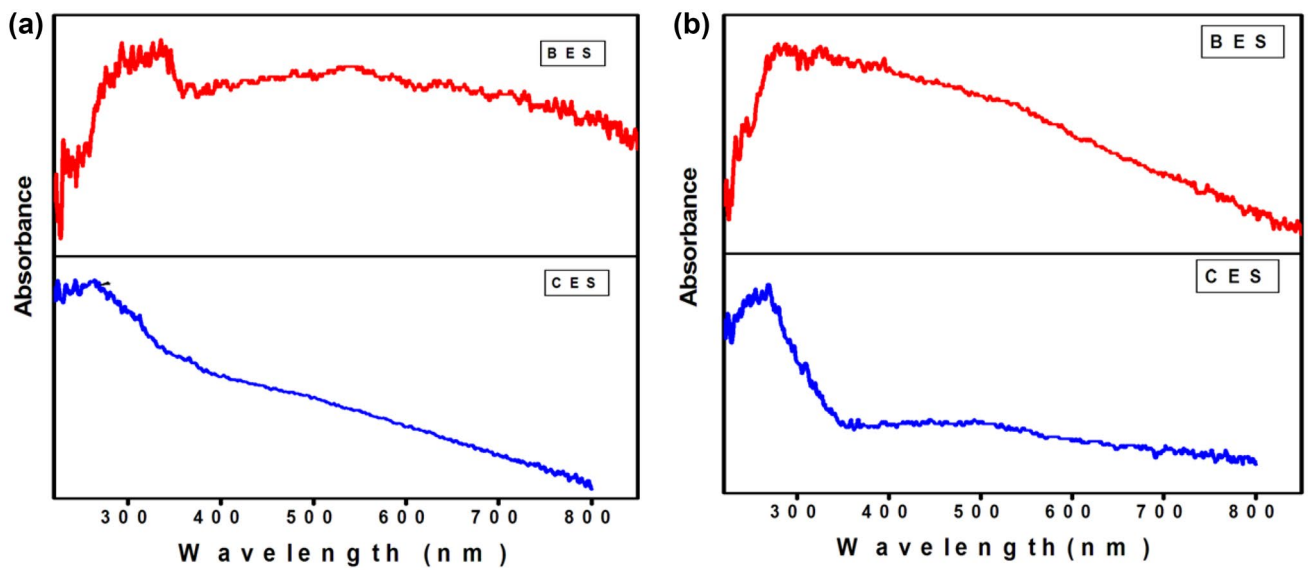


Fig. 7 UV-DRS spectra of Ac from **a** BES and **b** CES for 4:1 and 4:2 ratio

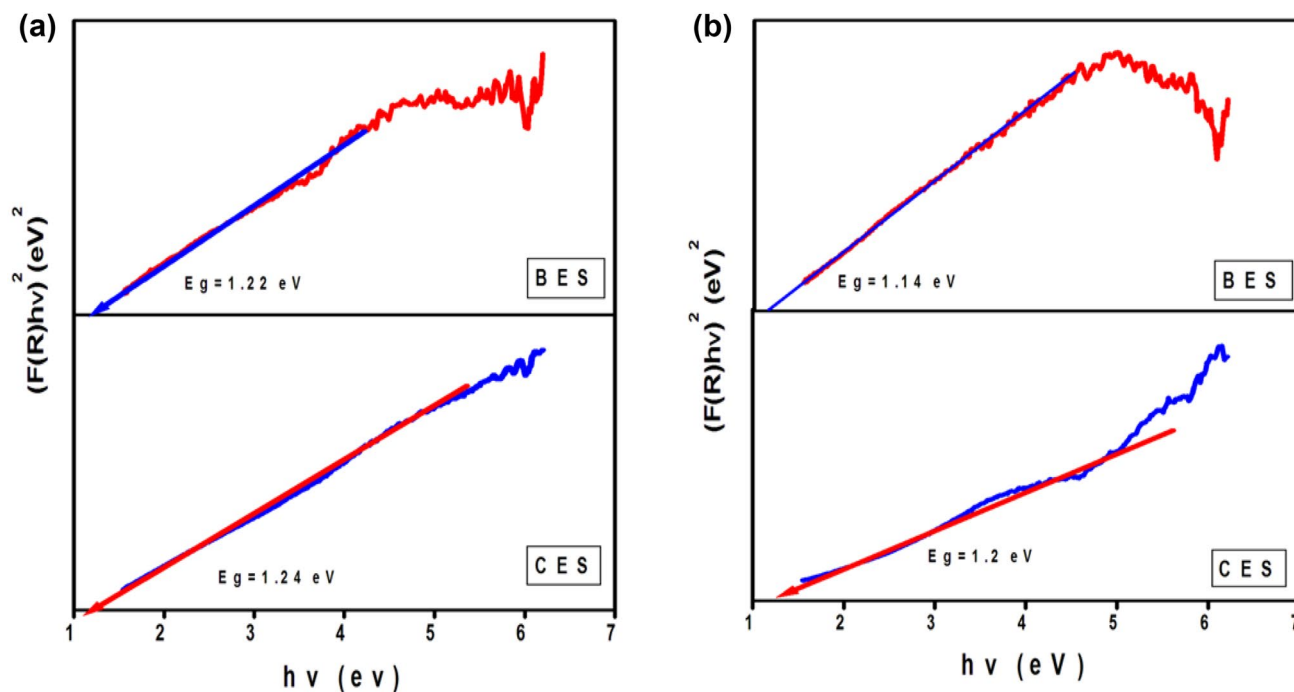


Fig. 8 Bandgap plot of Ac from BES and CES particles for **a** 4:1 and **b** 4:2 ratio

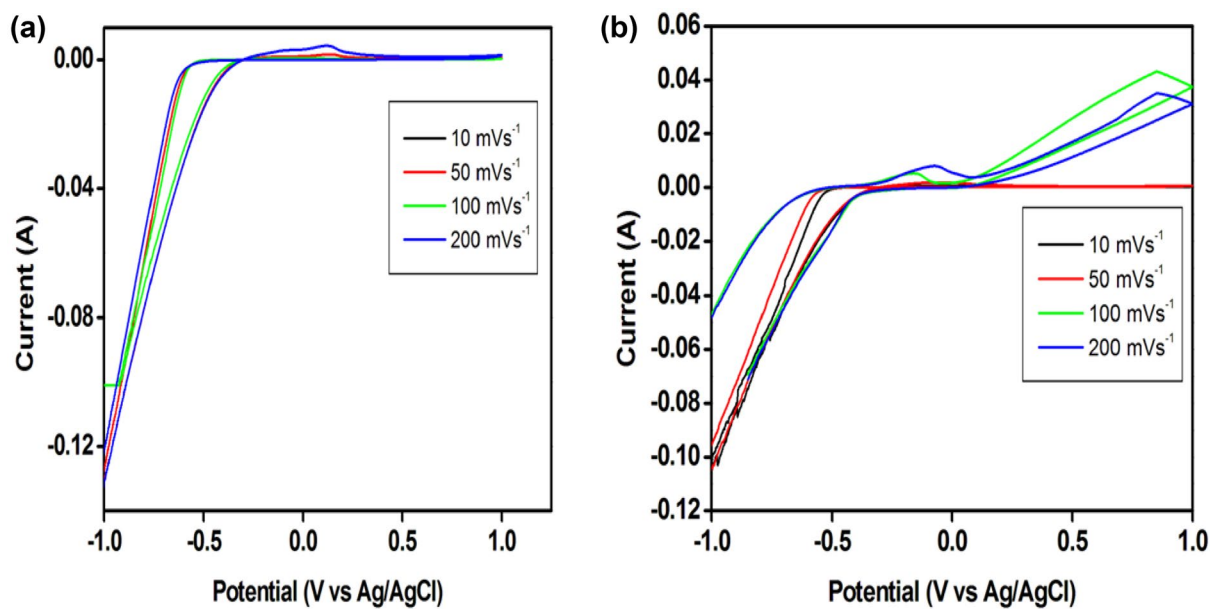


Fig. 9 CV plot of Ac from **a** BES and **b** CES for 4:1 concentration



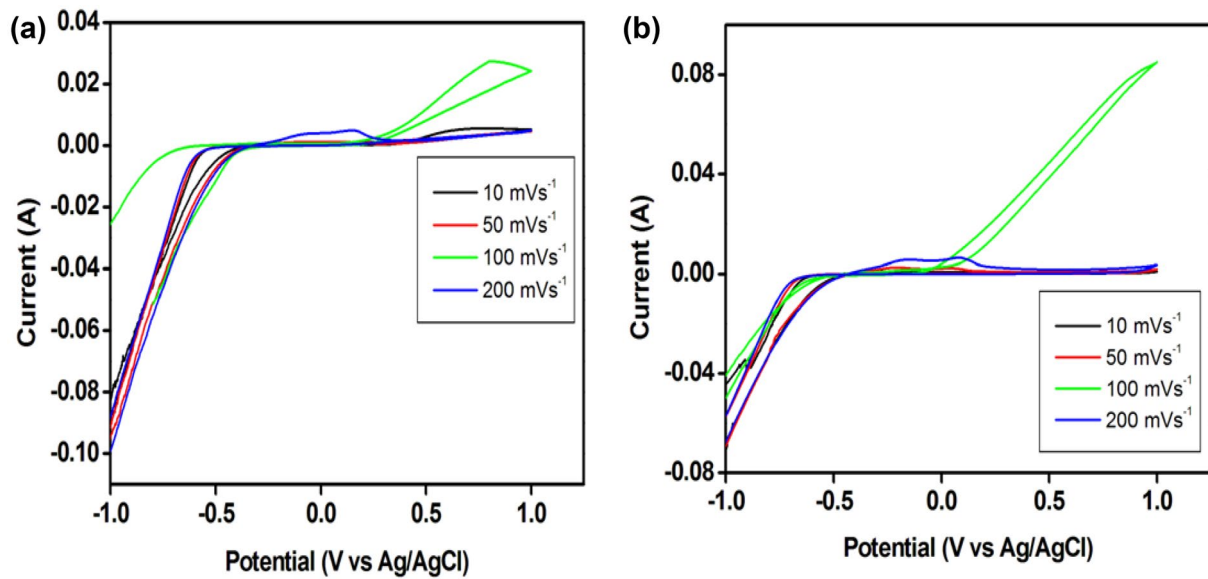


Fig. 10 CV plot of AC from BES and CES for 4:2 concentration

the material as witnessed by XRD and SEM analysis respectively.

### 3.3 Cyclic voltammetry (cv)

Figures 9 and 10 shows the CV curves of BES and CES for 4:1 and 4:2 concentration respectively. It is observed that the sample recorded at 10 mV/s exhibited higher integrated area since the particle seems to be highly dense. By using the CV curve the following parameter specific capacitance  $C_s$  can be calculated from Eqs. 6 and 7 as

$$C_a = I / [dv/dt] \times S \text{ (m F/cm}^2\text{)} \tag{6}$$

$$C_{sp} = C_a / \text{mass of sample} \tag{7}$$

where  $C_a$  is the areal capacitance (F),  $I$  is the integrated area of the CV curve,  $dv/dt$  is the scan rate and  $S$  is the surface area of the electroactive material. The variation of areal capacitance ( $C_a$ ) and specific capacitance ( $C_{sp}$ ) was calculated with respect to the different scan rates of the

working electrode as tabulated in Table 4. When the scan rate increases, the  $C_{sp}$  value gets decrease. The largest current in the BES sample revealed the excellent charge propagation in the electrodes. It is attributed to the electric double layer capacitor (EDLC) behavior. The narrow loop is due to larger resistance occurred in the samples due to the electrode/electrolyte interface. The irregular shape of the CV curve is due to water content, redox groups such as hydroxide group and carboxyl group [29, 30].

It is observed from Table 3 that the highest  $C_{sp}$  value is found about 155.8 F/g at 10 mV/s for BES which is due to higher areal capacitance. Similarly, CES has the highest  $C_{sp}$  value of 144.83 F/g at a scan rate of 10 mV/s that also indicates the enhanced capacitive performance. By comparing the results, the AC prepared from BES shows higher specific capacitance value.

By comparing the plots of 4:2 with 4:1 concentration, the loop of 4:2 is in a similar trend to that of 4:1 (BES and CES), however, the magnitude of the integrated area is slightly varied (lower). It may be attributed to higher  $CaCO_3$  content formed during activation. As similar in the

Table 4 Different scan rates, areal capacitance ( $C_a$ ) and specific capacitance ( $C_{sp}$ )

Scan rate (mV/s)	BES				CES			
	$C_a$ (mF/cm <sup>2</sup> )		$C_{sp}$ (F/g)		$C_a$ (mF/cm <sup>2</sup> )		$C_{sp}$ (F/g)	
	4:1	4:2	4:1	4:2	4:1	4:2	4:1	4:2
10	9.31	8.20	155.80	133.95	6.69	4.62	144.83	66.37
50	2.24	2.16	37.33	19.94	1.61	1.53	26.83	8.04
100	7.69	5.92	128.22	90.91	0.10	0.09	1.73	1.42
200	5.47	1.46	27.37	6.72	0.23	0.12	3.91	2.32

case of 4:1 ratio,  $C_s$  values found in 4:2 ratio are higher for both BES and CES for the scan rate of 10 mV/s. From the analysis, 4:1 is found to be an optimum ratio for obtaining an efficient high performance energy storage device. Hence, the result suggests that a better activated carbon material identified from eggshell waste which is suitable for energy storage application.

### 3.4 Electrochemical impedance spectra

Figure 11 shows the EIS plot of BES and CES for 4:1 concentration. These measurements were employed to examine the performance of the working electrode (Ac) using a three-electrode cell in 0.5 M  $H_2SO_4$  at the frequency range from 1 to 10 kHz versus the Ag/AgCl reference electrode. The EIS measurement shows semicircle nature for all the samples. From the equivalent circuit, R, C, and L values are found and it is given in Table 5.

The x-intercept at the beginning of the semicircle represents the equivalent series resistance including the electrolyte resistance, contact resistance at the interface between the electroactive material and substrate. The arc for the very high frequency corresponds to the charge transfer limiting process and was ascribed to the double layer capacitances in parallel with the charge transfer resistance at the contact interface between the

**Table 5** R, C and L values for 4:1 concentration of BES and CES

	BES	CES
$R_s$ ( $\Omega$ )	4.43	9.98
$R_{ct}$ ( $\Omega$ )	35.11	83.39
L	5.295E-8	5.275E-8
C	9.832E-5	7.779E-5

electrode and electrolyte solution [31]. By comparing BES and CES, the sample BES shows the lowest value of  $R_s$  and  $R_{ct}$  value which indicates higher conductivity and better charge transport of electrolyte ion.

Figure 12 shows the EIS plot of BES and CES for 4:2 concentration. In the EIS of BES (Table 5) the charge transfer resistance  $R_{ct}$  value get increased than 4:1 concentration, while it is lower than that of CES for 4:1 and 4:2. The R, C, and L values for BES and CES for 4:2 concentration are given in Table 6.

The results clearly reveal that type of eggshell waste, as well as the content of the activation agent, plays a prominent role in identifying energy storage materials. By comparing the results of  $R_s$  and  $R_{ct}$  of BES (4:1 and 4:2) with CES, the BES shows lower values. Hence, it can be concluded from the analysis that BES found to be a potential material for energy storage devices.

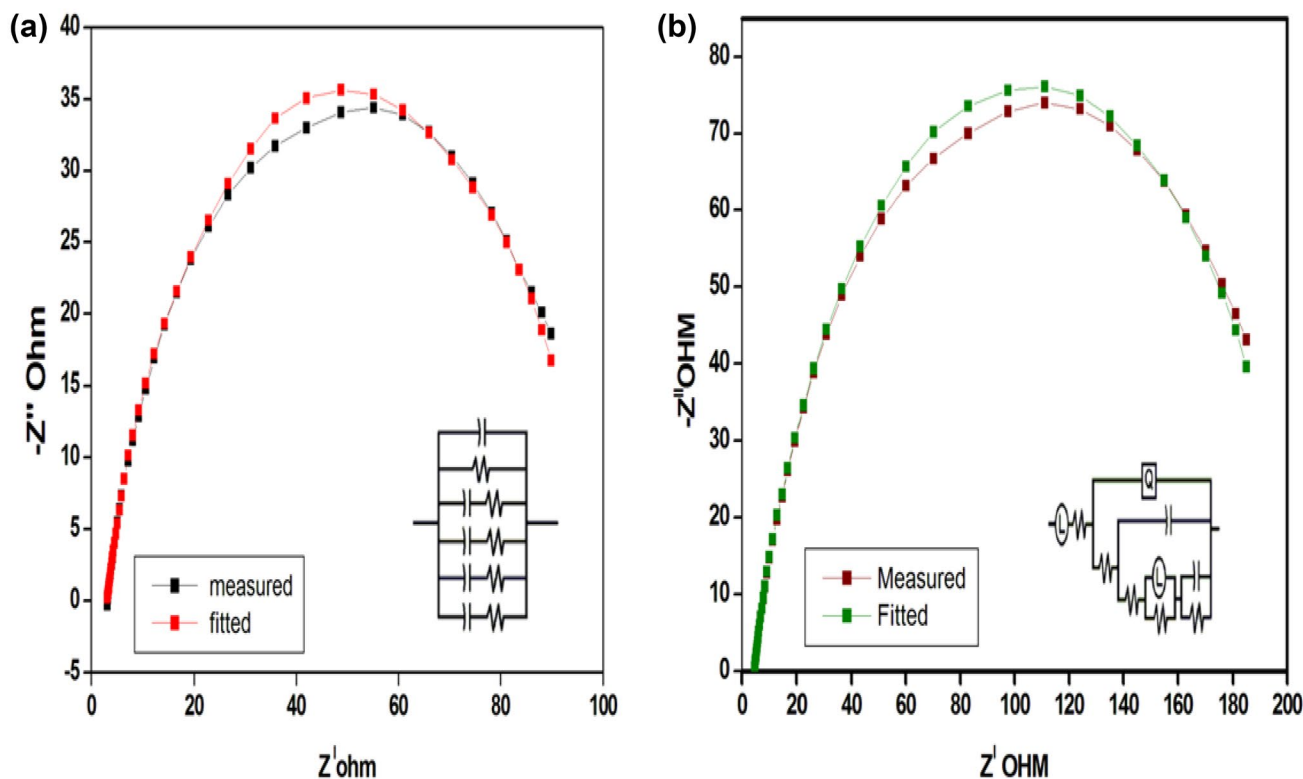


**Fig. 11** Nyquist plot of ac from **a** BES and **b** CES at 4:1 and its equivalent circuit

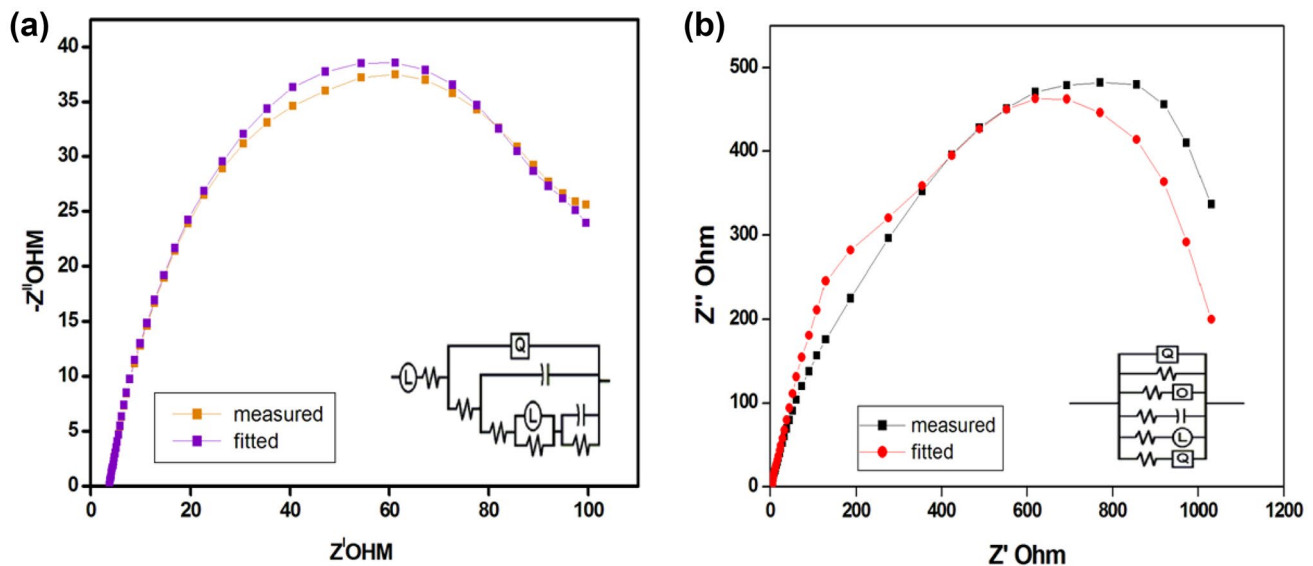


Fig. 12 Nyquist plot of ac from **a** BES and **b** CES at 4:2 and its equivalent circuit

**Table 6** R, C and L values for 4:2 concentration of BES and CES

	BES	CES
$R_s$ ( $\Omega$ )	9.58	10.26
$R_{ct}$ ( $\Omega$ )	53.39	127.42
L	4.985E-8	4.995E-8
C	7.123E-5	6.174E-5

## 4 Conclusion

In the study, activated carbon was prepared using broiler hen eggshell and Country hen eggshell for 4:1 and 4:2 concentrations of  $H_3PO_4$ . The XRD pattern confirmed the hexagonal structure of AC observed with peak shift, single and multi-crystalline structure. From the FTIR spectra, the presence of vibrational bands of CES is identical to BES, with slight variation observed in the intensity of the peaks. From UV-Vis DRS analysis, BES exhibited strong absorption in the visible region in comparison to CES. The bandgap values of BES and CES are almost identical to each other. Interestingly, the surface morphology reveals the irregular shape and size of particles observed for BES which are dense and porous nature while CES shows less dense with particular geometrical shape of the particles. It could be attributed to the influence of activating agent  $H_3PO_4$  on the different types of eggshells. From the CV analysis, the sample BES has achieved a higher specific capacitance value of 156 F/g compared to CES as supported by the EIS measurements that BES has the lowest  $R_s$  and  $R_{ct}$  values and hence exhibited better conductivity and charge storage. From the proximate

analysis ash content, moisture content, specific gravity, bulk density, and porosity can be calculated.

**Acknowledgements** The authors acknowledge DST-SERB, New Delhi for providing financial support under Extra Mural Research (F. No. EMR/2017/000351) fund. The author is grateful to Kalasalingam University for SEM analysis. The authors are thankful to the DST-FIST and UGC-SAP (DRS-I and II) for providing financial support to the Department of Physics, Manonmaniam Sundaranar University.

## Compliance with ethical standards

**Conflict of interest** The authors declare that they have no conflict of interest.

## References

- Rufford TE, Hulicova-Jurcakova D, Zhu Z, Gao Qing L (2008) Nanoporous carbon electrode from waste coffee beans for high performance supercapacitors. *Electrochem Commun* 10:1594–1597
- Zequine C, Ranaweera CK, Wang Z, Singh S, Tripathi P, Srivastava ON, Gupta BK, Ramasamy K, Kahol PK, Dvornic PR, Gupta RK (2016) High performance and flexible supercapacitors based on carbonized bamboo fibers for wide temperature applications. *Sci Rep* 6:31704
- González-García P, Centeno TA, Urones-Garrote E, Ávila-Brandé D, Otero-Díaz LC (2013) Microstructure and surface properties of lignocellulosic-based activated carbons. *Appl Surf Sci* 265:731–737
- Kalderis D, Bethanis S, Paraskeva P, Diamadopoulos E (2008) Production of activated carbon from bagasse and rice husk by a single-stage chemical activation method at low retention times. *Biores Technol* 99:6809–6816
- Rufford TE, Hulicova-Jurcakova D, Khosla K, Zhu Z, Gao Qing L (2010) Microstructure and electrochemical double-layer

- capacitance of carbon electrodes prepared by zinc chloride activation of sugar cane bagasse. *J Power Sources* 195:912–918
6. Foo KY, Hameed BH (2011) Utilization of rice husks as a feedstock for preparation of activated carbon by microwave-induced KOH and  $K_2CO_3$  activation. *Biores Technol* 102:9814–9817
  7. He X, Ling P, Qiu J, Moxin Yu, Zhang X, Chang Yu, Zheng M (2013) Efficient preparation of biomass-based mesoporous carbons for supercapacitors with both high energy density and high power density. *J Power Sources* 240:109–113
  8. Taer E, Deraman M, Talib IA, Awitdrus A, Hashmi SA, Umar AA (2011) Preparation of a highly porous binderless activated carbon monolith from rubberwood sawdust by a multi-step activation process for application in supercapacitors. *Int J Electrochem Sci* 6:3301–3315
  9. Zhang S, Shi X, Chen X, Zhang D, Liu X, Zhang Z, Mijowska E (2019) Large-scale and low-cost motivation of nitrogen-doped commercial activated carbon for high-energy-density supercapacitor. *ACS Appl Energy Mater* 6:4234–4243
  10. Bhomick PC, Supong A, Karmaker R, Baruah M, Pongener C, Sinha D (2019) Activated carbon synthesized from biomass material using single-step KOH activation for adsorption of fluoride: experimental and theoretical investigation. *Korean J Chem Eng* 4:551–562
  11. Sivachidambaram M, Judith Vijaya J, John Kennedy L, Jothiralingam R, Al-Lohedan HA, Munusamy MA, Elanthamilane E, Princy Merline J (2017) Preparation and characterization of activated carbon derived from the *Borassus flabellifer* flower as an electrode material for supercapacitor applications. *RCS New J Chem* 41:3939–3949
  12. Li Z, Zhang L, Amirkhiz BS, Tan X, Zhanwei X, Wang H, Olsen BC, Holt Chris MB, Mitlin D (2012) Carbonized chicken eggshell membrane with 3D architectures as high performance electrode. *Adv Energy Mater* 2:431–437
  13. Meng X, Deng D (2016) Trash to treasure: waste eggshells used as reactor and template for synthesis of  $Co_9S_8$  nanorod arrays on carbon fibers for energy storage. *Chem Mater* 28:3897–3904
  14. Alcaraz-Espinoza JJ, Pinto C, de Melo H, de Oliveira P (2017) Fabrication of highly flexible hierarchical polypyrrole/carbon nanotube on eggshell membranes for supercapacitors. *ACS Omega* 2:2866–2877
  15. Yang P, Xie J, Zhong C (2018) Biowaste-derived three-dimensional porous network carbon and bioseparator for high-performance asymmetric supercapacitor. *ACS Appl Energy Mater* 1:616–622
  16. Ekpete OA, Horsfall MJNR (2011) Preparation and characterization of activated carbon derived from fluted pumpkin stem waste. (*Telfairia occidentalis* Hook F). *Res J Chem Sci* 3:10–17
  17. Cree D, Rutter A (2015) Sustainable bio-inspired limestone eggshell powder for potential industrialized applications. *ACS Sustain Chem Eng* 3:941–949
  18. Mopoung S, Jitchajaroenkul K (2017) Characterization of activated carbon from eggshell membranes prepared using sodium acetate and zinc metal activation. *Am J Appl Sci* 14:737–747
  19. Durai G, Kuppusami P, Viswanathan K (2018) Investigation on microstructure and improved supercapacitive performance of Mn-doped CuO thin films prepared by reactive radio frequency magnetron sputtering. *J Mater Sci Mater Electron* 29(3):2051–2058
  20. Carvalho J, Araujo J, Castro F (2011) Alternative low-cost adsorbent for water and wastewater decontamination derived from eggshell waste: an overview. *Waste Biomass Valorization* 2:157–167
  21. Tangboriboon N, Kunanuruksapong R, Sirivat A (2012) Preparation and properties of calcium oxide from eggshells via calcination. *Mater Sci Pol* 30:313–322
  22. Corrêa THA, Holanda JNF (2016) Calcium pyrophosphate powder derived from avian eggshell waste. *Cerâmica* 62:278–280
  23. Salma K, Borodajenko N, Plata A, Berzina-Cimdina L, Stunda A (2008) Fourier transform infrared spectra of technologically modified calcium phosphates. In: 14th Nordic-Baltic conference on biomedical engineering and medical physics, pp 68–71. Springer, Berlin
  24. Borhade AV, Kale AS (2017) Calcined eggshell as a cost-effective material for the removal of dyes from aqueous solution. *Appl Water Sci* 7:4255–4268
  25. Al-Ghouthi MA, Salih NR (2018) Application of eggshell wastes for boron remediation from water. *J Mol Liq* 256:599–610
  26. Ahmed S, Ahmed A, Rafat M (2018) Supercapacitor performance of activated carbon derived from rotten carrot in aqueous, organic and ionic liquid-based electrolytes. *J Saudi Chem Soc* 8:993–1002
  27. Sixiao H, Hsieh Y-L (2014) Preparation of activated carbon and silica particles from rice straw. *ACS Sustain Chem Eng* 2:726–734
  28. Ummartyotin S, Tangnorawich B (2015) Utilization of eggshell waste as raw material for the synthesis of hydroxyapatite. *Colloid Polym Sci* 293:2477–2483
  29. Natalia M, Sudhakar YN, Selvakumar M (2013) Activated carbon derived from natural sources and electrochemical capacitance of double layer capacitor. *Indian J Chem Technol* 20:392–399
  30. Li Z, Zhanwei X, Tan X, Wang H, Holt CM, Stephenson T, Olsen BC, Mitlin D (2013) Mesoporous nitrogen-rich carbons derived from protein for ultra-high capacity battery anodes and supercapacitors. *Energy Environ Sci* 6:871–878
  31. Liu X, Yin C, Yang J, Liang M, Wei J, Zhang Z, Wang H, Wang Q (2016) Controllable preparation of an eggshell membrane supported hydrogel electrolyte with thickness-dependent electrochemical performance. *J Mater Chem A* 46:17933–17938

**Publisher's Note** Springer Nature remains neutral with regard to jurisdictional claims in published maps and institutional affiliations.